Frequency Measurement and Accuracy Evaluation of KRISS-1

KRISS Korea Research Institute of Standards and Science

This document is to provide the results of evaluations of an optically pumped atomic beam frequency standard, named KRISS-1, for the contribution to TAI as a new primary frequency standard (PFS) to meet the requirement of CCTF Recommendation CCTF/06-08 on the first report of a new PFS.

KRISS-1 is being operated by Length and Time Metrology Center of Korea Research Institute of Standards and Science in Daejeon, Korea.

Nov. 28, 2008.
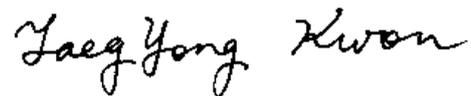
Taeg Yong Kwon, Ph.D.
Chief, Length and Time Metrology Center,
Division of Physical Metrology
Email: tykwon@kriss.re.kr

* This document was revised on Dec. 30, 2008 in accordance with the WGPFS comments.
* A couple of mistakes on writing down values were fixed on Jan. 6, 2009.

1. Frequency measurement of KRISS-1

Frequency measurement and accuracy evaluation of KRISS-1 was performed three times over the 15 day period of MJD 54654 to 54669, the 10 day period of MJD 54699 to 54709, and the 20 day period of MJD 54719 to 54739 (from Jul. 7 to Sep. 30, 2008).

1) MJD 54654 – 54669

- cycle duty: 99 %

Frequency difference [KRISS-1 – H1*]	1.370×10^{-12}	Link uncertainty $u_{\text{link/lab}}$	$< 1 \times 10^{-15}$
Frequency difference [UTC – H1]	1.373×10^{-12}	Link uncertainty $u_{\text{link/TAI}}$	$< 1 \times 10^{-15}$
		Type B uncertainty u_{B}	9.5×10^{-15}
		Type A uncertainty u_{A}	3×10^{-15}
Frequency difference [KRISS-1 – UTC]	-3×10^{-15}	Combined uncertainty u_{c}	1.0×10^{-14}

* H1: H-maser

2) MJD 54699 – 54709

- cycle duty: 99 %

Frequency difference [KRISS-1 – H1]	1.360×10^{-12}	Link uncertainty $u_{\text{link/lab}}$	$< 1 \times 10^{-15}$
Frequency difference [UTC – H1]	1.359×10^{-12}	Link uncertainty $u_{\text{link/TAI}}$	$< 1 \times 10^{-15}$
	-	Type B uncertainty u_{B}	9.5×10^{-15}
	-	Type A uncertainty u_{A}	4×10^{-15}
Frequency difference [KRISS-1 – UTC]	1×10^{-15}	Combined uncertainty u_{c}	1.0×10^{-14}

3) MJD 54719 – 54739

- cycle duty: 99 %

Frequency difference [KRISS-1 – H1]	1.362×10^{-12}	Link uncertainty $u_{\text{link/lab}}$	$< 1 \times 10^{-15}$
Frequency difference [UTC – H1]	1.358×10^{-12}	Link uncertainty $u_{\text{link/TAI}}$	$< 1 \times 10^{-15}$
	-	Type B uncertainty u_{B}	9.5×10^{-15}
	-	Type A uncertainty u_{A}	2×10^{-15}
Frequency difference [KRISS-1 – UTC]	4×10^{-15}	Combined uncertainty u_{c}	1.0×10^{-14}

2. Accuracy evaluation of KRISS-1

We ultimately measure f_K, which is the frequency of KRISS-1 seen by our hydrogen maser (H1). In our measurement, the uncertainties in f_K are classified by two types: the statistical uncertainty (type-A) in the frequency measurement that is the Allan's deviation in long term, and the systematic uncertainty (type-B) in determining the various frequency biases other than the end to end phase bias. The overall performance is defined by the combined standard uncertainty of those two.

2.1 Uncertainty budget

2.1.1 Quadratic Doppler Bias

The quadratic Doppler bias is determined from the atomic velocity profile, which is accurately obtained using our regularized inverse method [1]. Throughout the measurement, the Caesium (Cs) oven temperature was maintained at 100 °C. A typical value of the fractional frequency shift is -38±0.1 ×10^{-14}. We find that, the type-B uncertainty in this measurement is less

than 0.3 % and the uncertainty due to white noise is about 0.1 %. Here the uncertainty is mostly caused by the evanescent field at the beam hole of our short cavity (36 cm in length).

2.2.2 Quadratic Zeeman Bias

In KRISS-1, the digital servo measures the Zeeman frequency periodically by finding the center frequencies of m = ±1 transitions during the frequency stabilization routine. Afterwards, the Zeeman frequency shift is calculated and then continuously subtracted from the center frequency. Typically we measure the fractional frequency shift of 48581.5×10^{-14}, and when the frequency shift is compensated every half an hour, the associated uncertainty is less than $\times 10^{-15}$.

2.2.3 Rabi Pulling Bias

From the transit time distributions of atoms at the Zeeman sublevels, we numerically calculate the slope of the background signal from the neighboring Rabi pedestals and evaluate the Rabi pulling shift. We measure the fractional frequency bias of -0.35×10^{-14}. The uncertainty mainly arises from white noise in the transit time distribution, which is typically about 1×10^{-15}.

2.2.4 Cavity Pulling Bias

The cavity bias is obtained from the detuning slope of the cavity response curve and the numerical calculation of the transit time distribution curve. In KRISS-1, the fractional frequency difference is $-4.6(7) \times 10^{-15}$. The associated uncertainty of 0.07×10^{-14} is caused by the statistical noise in the transit time distribution and the Rabi frequencies.

2.2.5 End-to-end Cavity Phase Bias

The beam reversal technique has been used to measure the end-to-end phase difference. KRISS-1 is oriented such that the atoms propagates from east to west direction (or from west to east depending on which Cs oven is activated) to minimized the effect of the earth magnetic field. Since the change of the beam direction induces sign changes for the phase difference, the frequency shift can be evaluated by taking a weighted average of the frequency measurements.

During normal operation, we typically measure the frequency bias of 1.171 ×10^{-14} (east to west) and 1.130 ×10^{-14} (west to east) with an uncertainty of 4.1 ×10^{-15}.

2.2.6 Bloch-Siegert Bias

When the Cs oven temperature and the modulation depth are set at 100 °C and 120 Hz respectively, we obtain the optimal Rabi frequency of about 34.0 krad/s. Accordingly, the shift of the Rabi pedestal is 0.796 mHz, and the corresponding frequency shift in Ramsey fringe is 34 μ Hz. Overall, we measure the fractional frequency of 0.37 ×10^{-14} with an uncertainty of 0.002 ×10^{-14}.

Table 1: Frequency Biases and relevant type-B Uncertainty

Physical Effect	Bias (×10^{-14})	Uncertainty (×10^{-14})
Quadratic Zeeman	48581.5	0.1
Quadratic Doppler	-38.02	0.1
Cavity Pulling	-0.46	0.07
Bloch-Siegert	0.37	0.002
Rabi Pulling	-0.35	0.1
Gravitation	0.9	0.1
Blackbody Radiation	-1.66	0.02
End to end Cavity Phase	117.1 (east to west) 113.0 (west to east)	(Type-A) 0.41
Light Shift	0	0.9
Majorana	0	0.2
C-field Inhomogeneity	0	0.05
Ramsey Pulling	0	0.01
Distributed Cavity Phase	0	0.1
Combined		**1.0**

2.2 Frequency Stability

Fig. 1 shows the Allan deviation of the frequency difference between KRISS-1 and the reference hydrogen maser (H1). During normal operation, KRISS-1 shows a short term frequency stability of $1.3 \times 10^{-12}/\sqrt{\tau}$.
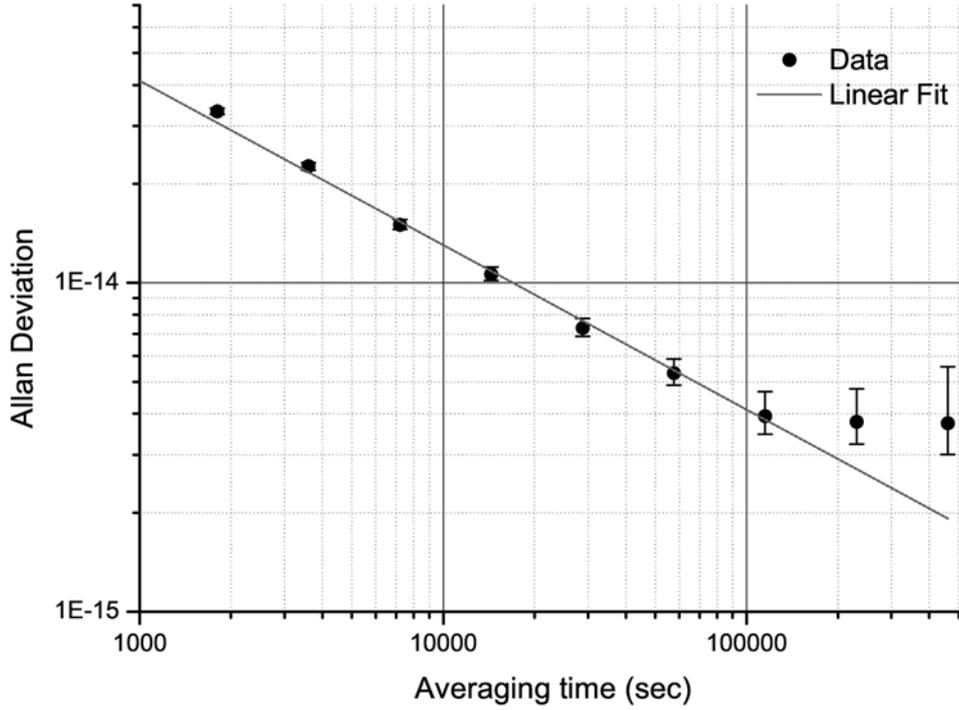
Fig. 1: Allan deviation of the frequency difference between KRISS-1 and the reference maser

2.3 Time Difference Measurement

From July to September of 2008, three sets of accuracy evaluations have been performed. During the same periods, the frequency deviation between our reference H-maser and UTC has also been measured, which can be found in Circular T of BIPM. Using these data, we compared the frequency difference between UTC and our reference H-maser to the frequency difference between KRISS-1 and the maser for three separate occasions: MJD 54654-54669, 54689-54709 and 54719-54739.

We first measure the frequency difference between KRISS-1 and the reference maser: It is obtained via the data acquisition of KRISS-1. Simultaneously, the frequency difference between the maser and UTC(KRISS) is acquired from our internal time comparison data. Furthermore, the frequency difference between UTC and UTC(KRISS) is obtained from the monthly updated Circular T.

That is:

$$f_1 = f_{KRISS-1} - f_{H-maser} = f_K$$
$$f_2 = f_{UTC(KRISS)} - f_{H-maser} \qquad \text{Eq. (1)}$$
$$f_3 = f_{UTC} - f_{UTC(KRISS)}$$

Ultimately, the comparison between the frequency difference of UTC with respect to KRISS-1 is achieved by comparing f_1 to $f_2 + f_3$. For its result, refer to section 1 (Frequency measurement of KRISS-1) of this document.

* A detailed description of KRISS-1 and its uncertainty evaluation is given in the attached file of "*MetrolgiaSubmission_KRISS-1.PDF*" which is a manuscript submitted to Metrologia for publication on Nov. 12, 2008. The manuscript was revised on Dec. 30, 2008 in accordance with the WGPFS comments. The revision will be reflected in the last version of the paper.

Reference

[1] Y.H. Park, S.H. Lee, S.E. Park, and H.S. Lee and T.Y. Kwon, *Applied Physics Letter* **90**, 174112 (2007).

Accuracy Evaluation of an Optically Pumped Caesium Beam Frequency Standard KRISS-1

SooHeyong Lee[1], Young-Ho Park[2], Sang Eon Park[1], Ho Seong Lee[1], Sung Hoon Yang[1], Dai-Hyuk Yu[1], and Taeg Yong Kwon[1,*]

[1]Korea Research Institute of Standards and Science, Daejeon 305-600, Republic of Korea

[2]Quantum Optics Laboratory, Advanced Photonics Research Institute, GIST, Gwangju 500-712, Republic of Korea

E-mail: `tykwon@kriss.re.kr`

Abstract. We report on the Korea's first optically pumped primary frequency standard (KRISS-1) developed at the Korea Research Institute of Standards and Science. Although a relatively small microwave cavity (cavity drift region is about 36 cm in length) has been employed in this experiment, we achieved our desired frequency accuracy by applying the regularized inverse on the Ramsey spectrum analysis and compensating the effect of evanescent field inside the cavity. KRISS-1 typically performs at a short term stability of $1.3 \times 10^{-12}/\sqrt{\tau}$ with a combined uncertainty of 1.0×10^{-14}.

1. Introduction

Primary frequency standard (PFS) has important applications in various aspects of modern society. For example, it is used to generate accurate time, calibrate global positioning systems and construct elaborate telecommunication networks. It also provides useful tools for studying fundamental principles of science such as verifying theory of relativity [1], measuring constancy of fine structure constants [2] and probing properties of pulsar in outer space [3]. Many laboratories including Korea Research Institute of Standards and Science (KRISS) are involved in the development of various types of PFS. We commenced building an optically pumped frequency standard (KRISS-1) at the KRISS Length/Time metrology group in 1988 to achieve an accuracy of 10^{-13}; Nevertheless our ultimate goal was later adjusted to 10^{-14} level after implementing various hardware and software improvements in 1998. Although a relatively short Ramsey cavity is installed in KRISS-1 [4], by developing a regularized inverse method [5] to analyze Ramsey spectra and accounting for the contributions from evanescent field at the cutoff guide of the cavity [6], we were able to accurately evaluate important frequency shifting parameters that are induced by various physical phenomena along with their uncertainties. In this paper, we report on the details of our accuracy evaluation, of which result has been compared to the Circular-T data during past three months. In near future, we expect that some of the theoretical and experimental approaches developed in this work are expected to be used in the evaluation of our upcoming atomic fountain clock [7, 8].

2. Description of KRISS-1

2.1. Atomic Beam Tube

Fig. 1 shows the overall design of KRISS-1. Inside the cylindrical atomic beam tube, there are several core components that comprise the optically pumped atomic clock such as Ramsey cavity, static magnetic field rods, fluorescent collector, magnetic shield and so on. At each end of the atomic beam tube, two cesium (Cs) ovens are installed. The vacuum inside the chamber is pumped by two 400 L/s ion pumps and one 1200 L/s non-evaporable getter pump and it is maintained at about 1×10^{-6} Pa. 4 AR-coated infrared view ports are placed on the chamber for the delivery of pump and detection lasers. Several electrical-feedthroughs are also attached on the chamber to send static currents or to receive fluorescent signals from inside. Temperature and humidity of the experimental hall are maintained at 23.5 C° and 40 % respectively by an air-conditioning (AC) unit that is isolated from the rest of AC systems in the building. In KRISS-1, Cs ovens are comprised of a copper pinch tube that holds Cs ampule in vacuum, and it is wrapped by heating wire. Six thermo-sensors monitor the temperature at various parts of the ovens, and proportional-integral circuits are used to stabilize the temperature within ±0.1 C°. Between the ovens and the atomic beam tube, beam collimators are installed. The outer dimension of each collimator cross-section is 8.3×7.4 mm^2 and it is filled 23 stainless steel tubes whose diameter is about 1.6 mm and 10 cm in length. Under normal operation, the temperature of the oven is maintained at 100 C° while the collimator is kept at 120 C°.

2.2. Microwave Cavity

A correct design of the microwave cavity minimizes various sources of frequency shifts. In our experiment, E-plane type Ramsey cavity is used, of which length is 36 cm

from one end of the interaction region (each 1 cm in length) to the other. Here the dimension of the wave guide is determined such that only TE_{10} mode may propagate inside the cavity: the cross-section of the guide is about 10×22.6 mm^2. Beam holes are carved on each end surface of the cavity. They are precisely machined to conform to the cutoff guide design to inhibit microwave leakage. The dimension of the cutoff guide is 3×3 mm^2 which is sufficiently smaller than the wavelength of the microwave at 9.2 GHz. The Ramsey cavity is made from oxygen free high conductivity copper. Despite high conductivity of the material, the amplitude of the electric field propagating inside the cavity decreases along the direction of the wave guide because the electrical current dissipates by generating heat. Before installing the cavity inside the beam tube, resonance frequency of the cavity is measured via the reflected power method [9]. For KRISS-1, its resonance frequency measured in vacuum is 2.95 MHz higher than the frequency measured in air. Quality factor of the cavity is about 1800 and the resonance frequency is tuned such that it matches the clock transition frequency within 200 kHz. A hydrogen maser, which keeps a traceability with TAI, works as a reference oscillator for our 9.2 GHz microwave source. The maser initially produces a 10 MHz signal that is sent to a low noise distribution amplifier (Symmerticom FTS 6502). The signal is then re-distributed to a frequency synthesizer (Agilent E8247C with a low noise option), which generates 9.2 GHz with a fine tuning of 0.001 Hz without loss in resolution. The microwave from the synthesizer output goes through a voltage-controlled attenuator and it is subsequently divided into two parts via a power splitter. One of the divided output is directly sent to the atomic beam tube while the other is fed into a commercial power meter. Reading from the meter is used as a feedback to keep the microwave power fixed at a constant level. The output control resolution (0.02 dB) is ultimately limited by the sensitivity of the power meter. During the operation, the slow square-wave frequency

modulation technique is used to locate the center frequency of the Ramsey spectrum.

2.3. Laser System

Nearby the atomic beam tube, our laser system is built on a separate optical table (See Fig. 2). In detail, we use a compact extended cavity diode laser developed by the time metrology group at KRISS [10], which is frequency locked to Cs D_2 line. By installing Littman grating external cavity to a commercial semiconductor laser, we narrowed the line-width of the laser from 37 MHz to 200 kHz. Here it is very crucial that the frequency lock scheme is robust and reliable enough to withstand the noise in laser frequency and output power. In the master laser schematics of Fig. 2, the frequency of the external cavity diode laser is stabilized to the crossover resonance line between F=4 to F'=4 and F=4 to F'=5 transitions via the modulation transfer spectroscopy, in which the modulation frequency is kept at 7 MHz. The modulation coefficient and phase shift values for the electro-optic modulator are controlled by a direct digital synthesizer. As can be seen in Fig. 2, a fraction of the output from the master laser is fed into the slave laser. Subsequently, the injection locked slave laser outputs an amplified laser beam that follows the frequency characteristics of the master laser. At this point, the injection locked slave laser outputs 100 mW that is divided into two via a polarization beam splitter. Inside the slave laser, F=4 $\rightarrow$ F=5 transition (for detection) is achieved by adding 125.5 MHz to the original master laser frequency via an acousto-optic modulator (AOM). Subsequently, F=4 $\rightarrow$ F=3 transition (for pumping) is attained by subtracting 226 MHz from the laser frequency by double passing an additional AOM. Finally the laser beams are delivered to the atomic beam tube via polarization maintaining optical fibers. Although the use of the optical fiber clears the spatial mode of the laser beam and insures a flexible delivery, the coupling efficiency deteriorates in time. And thus, a power stabilizing scheme has been implemented to keep the output power constant.

Polarization beam-splitter is installed in front of the view ports on the beam tube, so that only the horizontally polarized beam enters the atomic beam tube. After interacting with the atomic beam, the horizontally polarized beam goes through a quarter wave plate and then retro-reflected. At this point, the laser beam is vertically polarized and once again interacts with the atoms before it is detected by the photodiode outside the vacuum. The signal from the photodiode is proportional to the laser output power, and it is used to control the amplitude of the RF signal going into the AOM that ultimately maintains the laser power to a constant level. Fluoresce from the interacting atoms is collected by two concave mirrors. A graphite tube is installed along the drift region to reduce light scattering and unwanted interference with the microwave field. Finally a Si photodiode is installed inside the vacuum and a low noise amplifier is placed outside for the light detection.

3. Accuracy Evaluation Process of KRISS-1

A monthly accuracy evaluation begins on a modified Julian date (MJD) that ends in four or nine and continues throughout the month. However, prior to starting the evaluation, a few crucial parameters such as the optimal operating power and the slope of Ramsey spectrum at the modulation depth must be measured and set accordingly. For the data acquisition and analysis, we have developed a series of program routines to control various instruments using Labview programming language. And also, the frequency evaluation and Ramsey spectra analysis codes are developed by KRISS scientists and written in MATLAB. In our main acquisition routine, the input microwave frequency is initially set at approximately 120 Hz (modulation depth) away from the center. And then, the strength of the microwave is scanned from its minimum level until the Ramsey transition signal reaches the maximum. Once the optimal power is determined, the slope

of the Ramsey fringe at each modulation depth is measured. Using these information, the digital servo locates the center of Ramsey spectrum via the slow square wave frequency modulation method; subsequently, Ramsey spectra are taken at 7 Zeeman sublevels. The procedure is repeated for 2.5 dB below the optimal microwave power because the regularized inverse requires at least two Ramsey spectra taken at different microwave powers. Afterwards, centers of the Ramsey spectrum at the optimal power is monitored for half an hour. Once the Ramsey spectra and center frequencies are collected, they are analyzed by an independent analysis PC; meanwhile, the acquisition PC keeps collecting data simultaneously.

In the analysis, accurate deduction of Rabi-frequencies and transit time distribution (TTD) of atoms across the Ramsey cavity is required. Alaa Makdissi et al. [11] had previously adopted an inverse method to obtain TTD. In his method, given an accurate Rabi frequency value, the TTD is calculated from a single Ramsey spectrum. Shirley et al. [12] took a different approach where he measured Ramsey spectra at several different microwave powers and calculated the velocity distribution and the Rabi frequency by taking a weighted average. In our pevious work, a fourier transform based method was used to deduce TTD[13]. However, we have recently developed an alternative method to deduce accurate TTD and Rabi frequencies simultaneously by applying regularized inverse on Ramsey spectra measured at two different microwave powers [5]. It typically takes less than 10 s to deduce the Rabi-frequency and TTD using a PC capable of performing 9.6×10^8 floating point operations per second. The systematic uncertainty for finding a Rabi frequency in this method is about 0.02 %. However, in actual experiment, the uncertainty is limited by our microwave power feedack scheme. Using the regularized inverse method, the velocity distributions at 7 different transitions ($m = 0, \pm1, \pm2, \pm3$) are obtained (See Fig. 3). Different areas under different distribution curves implies that

there are slight variations in density of Cs atoms residing at each Zeeman sublevel. TTD from neighboring Ramsey spectra enable us to obtain correct shape of Rabi-pedestals of neighboring transitions and eventually calculate necessary frequency biases such as Rabi pulling shift. After the analysis, 7 frequency biases are calculated from the Ramsey spectra, of which details are discussed in later paragraphs. Those biases are subtracted from the averaged center frequency and then stored in a text file for a permanent record. Temperature and humidity inside the experimental hall and the vacuum level inside the beam tube are continuously monitored.

Table 1. Uncertainty Budget

Physical Effect	Bias $(\times 10^{-14})$	Uncertainty $(\times 10^{-14})$
Quadractic Zeeman	48581.5	0.1
Quadratic Doppler	-38.02	0.1
Cavity Pulling	-0.46	0.07
Bloch-Siegert	0.37	0.002
Rabi Pulling	-0.35	0.1
Gravitational	0.9	0.1
Blackbody Radiation	-1.66	0.02
End to End Cavity Phase	117.1 (east to west) 113.0 (west to east)	(Type-A) 0.41
Light Shift	0	0.9
Majorana	0	0.2
C-field Inhomogeneity	0	0.05
Ramsey Pulling	0	0.01
Distributed Cavity Phase	0	0.1
Combined		1.0

4. Frequency Biases

Table 1 shows the important frequency biases and the relevant type-B uncertainties that are evaluated in this work. All the tabulated parameters are normalized to the clock transition frequency (9 192 631 770 Hz). Among the biases for which corrections

are being made, the uncertainties in the end-to-end cavity phase difference is most dominant: We find that the optimized cavity design and precise machining are required to minimize it. Since a short cavity (36 cm from one interaction region to another) is installed in KRISS-1, it is very important to account for the presence of evanescent field inside the beam hole. Park et al. [6] recently demonstrated a method to compensate the effect of the evanescent field during the Ramsey spectrum analysis.

4.1. Quadratic Doppler

Resonance frequencies of atoms depend on their propagation velocity inside Ramsey cavity due to Doppler-effect [13, 14]. In KRISS-1, since atoms interact with standing wave and the direction of atomic beam is perpendicular to the microwave propagation, the first order Doppler-effect becomes negligible; Nevertheless, the second order contribution remains. A typical frequency shift due to the quadratic Doppler-effect is in order of a few mHz. It is one of the largest frequency biases that need to be compensated accurately in order to achieve the optimal performance of PFS. The frequency of the microwave ω observed by the atoms propagating at the velocity v is shifted by $\omega(1 + v^2/2c^2)$ where c is speed of light. Therefore, the quadratic Doppler shift is given as $-\nu_{\mathrm{hfs}}v^2/2c^2$, where ν_{hfs} is the unperturbed Cs hyperfine separation. Since this frequency shift is correlated to the atomic velocity profile, it needs to be weighted averaged with respect to TTD of atoms:

$$f_{\mathrm{qD}} = -\frac{\nu_{\mathrm{hfs}}L^2}{2c^2D}\int_0^\infty \frac{1}{T^2}(T + \partial\Theta/\partial\Delta_{\mathrm{m}})\sin^2(\Omega\tau)\sin(\Delta_{\mathrm{m}}T + \Theta)\rho(T)dT \quad (1)$$

with

$$D = \int_0^\infty (T + \partial\Theta/\partial\Delta_{\mathrm{m}})\sin^2(\Omega\tau)\sin(\Delta_{\mathrm{m}}T + \Theta)\rho(T)dT, \quad (2)$$

where $\Theta = 2\arg(\cos\frac{\Omega\tau}{2} + i\frac{\Delta_{\mathrm{m}}}{\Omega}\sin\frac{\Omega\tau}{2})$, $\Omega = \sqrt{\Delta_{\mathrm{m}}^2 + b^2}$ for the modulation amplitude of Δ_{m} and the Rabi frequency b. T and τ are the flight time of atoms across the drift

region with the length L and the interaction region respectively. For KRISS-1, the regularized inverse is used to obtain TTD from two Ramsey spectra that are measured at the optimal microwave power and -2.5 dB below the optimal power. Throughout the measurement, the Cs oven temperature was kept at 100 °C. A typical value of the fractional frequency shift is -38±0.1 $\times 10^{-14}$. We find that, the type-B uncertainty in our method, which is caused by the evanescent field at the cavity beam hole, is less than 0.3 % and the uncertainty due to white noise is about 0.1 %.

4.2. Quadratic Zeeman

A static magnetic field is applied inside the atomic beam tube to separate the degeneracy among Zeeman sublevels. However this causes a frequency shift that is proportional to the second order magnetic perturbation:

$$f_{qZ} = 8\nu_Z^2/\nu_{hfs}, \tag{3}$$

where ν_Z is the Zeeman frequency, which is defined as below:

$$\nu_Z = \frac{(g_J - g_I)\mu_B B_0}{8\pi\hbar}, \tag{4}$$

where g_J and g_I are g-factors for the atom and nucleus, μ_B is the Bohr magneton constant and B_0 is the static magnetic field inside the cavity. This frequency offset is always positive and independent of microwave power, modulation depth and TTD. Since the quadratic Zeeman shift carries the largest value among all the shifting parameters, ν_Z needs to be determined to the highest precision to minimize its uncertainty. The uncertainty mainly comes from the drift in the strength of the magnetic field. In our experiment, a low-noise power supply (Agilent 6625A) provides the current for generating the magnetic field. However, due to the intrinsic thermal characteristic of the device, the magnetic field slowly changes in long term, which results in a frequency drift due to the quadratic Zeeman effect. In KRISS-1, the digital servo measures the Zeeman

frequency periodically by finding the center frequencies of $m = \pm 1$ transitions during the frequency stabilization routine. Afterwards, the Zeeman frequency shift is calculated and subtracted from the center frequency. At a static current of 1 A, the Zeeman frequency is about 71 kHz and shows 0.0014 %/day drift in the magnetic field strength. When the frequency shift is compensated every half an hour, the associated uncertainty is less than 10^{-15}. If the magnetic field in the drift region is not homogeneous, above equation needs to be modified because the Zeeman frequency is determined by the mean magnetic field while the resonance frequency of the clock transition is determined from the root mean square of the field. Nevertheless, since the magnetic field inhomogeneity in the cavity region is less than 0.1 %, the shift due to the field inhomogeneity is less than 5×10^{-16}.

4.3. Rabi pulling

When the static magnetic field inside the beam tube is parallel to the oscillating magnetic field of the microwave, only the σ transitions are allowed. Here neighboring σ transitions have extensive Rabi pedestal tails that overlay on top of each other. And thus, an asymmetry in the amplitude of neighboring transition signals at $m = \pm 1$ leads to a shift in the observed clock transition frequency, which is known as Rabi pulling [15, 16, 17]. During the optical pumping process, atoms are mostly populated at the Zeeman sublevels of $F = 3$ state. Depending on the polarization direction of the pumping laser relative to the quantization axis, population densities at 7 Zeeman sublevels vary. In general, the asymmetry of the Zeeman spectrum is caused by not only the population difference between Zeeman sublevels but also a cavity mistuning. And thus, two different effects should be identified separately in order to calculate the Rabi pulling shift. Shirley et al. [14] used a leverage method, in which the pedestal offset frequency is measured to identify three physical effects: Rabi pulling, cavity

pulling, and magnetic field inhomogeneity. Our method is based on the regularized inverse applied to 7 Zeeman spectra. As can be seen in Fig. 3, we measure the atomic populations at the Zeeman sublevels not the amplitudes of Zeeman spectrum. From the transit time distributions of the sublevels, we numerically calculate the slope of the background signal from the neighboring Rabi pedestals and evaluate the Rabi pulling shift. The uncertainty mainly arises from white noise in the transit time distribution, which amounts to 1×10^{-15}.

4.4. Cavity Pulling

If the resonance frequency of the Ramsey cavity does not match the clock transition frequency, strength of the microwave built up inside the cavity varies for different detuning frequencies. In such instances, the Ramsey spectrum carries an asymmetry in its lineshape. As a result, when the center of the spectrum is found using the slow square wave frequency modulation method, it is shifted by an amount of

$$f_{\text{cav}} = -\frac{\partial S/\partial b}{\partial S/\partial f} \times \frac{db}{df} f_{\text{m}}. \tag{5}$$

Here, the partial derivative terms represent the differential coefficients for the transition signal with respect to both the Rabi frequency b and the detuning frequency f when the detuning frequency is set to the modulation amplitude $f_{\text{m}} = \Delta_{\text{m}}/2\pi$. db/df is the slope of the cavity response function at the clock transition frequency. In our work, the AC Zeeman method [18] was initially employed to find the cavity response function of KRISS-1. However, during the actual operation of the clock, an alternate method has been employed to periodically monitor the cavity response. The regularized inverse approach enables us to find Rabi-frequencies for 7 Zeeman sublevels with unprecedented accuracy (within 0.02 %) [6]. From those values and the transition strengths of the σ transitions, we can measure the frequency dependent microwave power buildup inside

the cavity [19]. Fig. 4 shows that data obtained via this method is in good agreement with the result from the AC Zeeman method. The cavity pulling shift is obtained from the detuning slope of the cavity response curve and the numerical calculation of the partial derivatives in Eq. (5) using TTD. In KRISS-1, the fractional frequency difference due to the cavity pulling is -4.6(7)×10^{-15}. The uncertainty comes from the statistical noise in the TTD and the Rabi frequencies.

4.5. Gravitational Shift

According to the theory of general relativity, a frequency shift of $gh\nu_{\mathrm{hfs}}/c^2$ is expected at the altitude difference of h [20, 21]. Since the reference altitude of the Universal Coordinated Time (UTC) is the mean sea level (i.e. the geoid), the frequency shift due to gravity can be compensated by accounting for the height from the sea level; Typically, 1.09×10^{-13} is expected per 1 km. The height difference between the geoid and the location of KRISS-1 is deduced from the global positioning system (GPS) antenna that is installed on the roof of the experimental building. From the GPS data, the ellipsoidal height of the GPS receiving antenna is calculated to be 123.6 m, and the difference between WGS84 and the geoid at our coordinate is 25.01 m. Consequently, the orthometric height of the antenna is 98.59 m. By measuring the height difference between the location of KRISS-1 and the GPS receiver, the orthometric height of KRISS-1 is measured to be 86.9 m within uncertainty of 1 %. The frequency bias of 9.48×10^{-15} is obtained. The uncertainty in this measurement is less than 1×10^{-15}.

4.6. Blackbody Radiation

Above the absolute zero temperature, the random perturbation field of the blackbody radiation causes an energy level shift through the electric dipole and magnetic dipole transitions. This particular shift is proportional to the square of the random thermal

radiation field. Since the spectral density is a function of temperature, the frequency shift due to blackbody radiation can be also given as a function of temperature:

$$f_{\mathrm{bl}} = -1.573 \times 10^{-4} W^4 (1 + 0.014 W^2), \tag{6}$$

where W is a unitless parameter, in which the ambient temperature in Kelvin is divided by 300 K. A possible uncertainty arises from temperature fluctuation and thermal drift inside the atomic beam tube:

$$\sigma_{\mathrm{bl}} = 6.292 \times 10^{-4} W^3 (1 + 0.021 W^2) \sigma_W. \tag{7}$$

The temperature inside the experimental hall is maintained at 23.5 °C within ± 1 °C, and the relative frequency shift due to blackbody radiation is -1.66×10^{-14} within the uncertainty of 2.2×10^{-16}.

4.7. End-to-end Cavity Phase

When the phases of the microwave field at two ends of the cavity are different, the center of the Ramsey fringe undergoes a frequency shift. Typically, this mismatch is caused by imperfect machining and the finite conductivity on the internal surface of the cavity. In our experiment, the beam reversal technique has been used to measure the end-to-end phase difference. KRISS-1 is oriented such that the atomic beam propagates from east to west direction (or from west to east depending on which oven is activated) to minimize the effect of the earth magnetic field. Since the change of the beam direction induces sign changes for the phase difference, the frequency shift can be evaluated by taking a weighted average of the frequency measurements. Given the phase difference ϕ, the frequency shift is expressed as

$$\begin{aligned} f_\phi &= -\frac{\phi}{2\pi D} \int_0^\infty \sin^2(\Omega\tau) \sin(\omega_{\mathrm{m}} T + \Theta) \rho(T) dT \\ &= -\phi F. \end{aligned} \tag{8}$$

Since F is a function of microwave strength, the modulation depth and TTD, it may differ by a few percent depending on the direction of the beam propagation. When the beam flows from east to west, the center of Ramsey spectrum, which is found after all other frequency biases are subtracted, is given as:

$$f_{\text{ew}} = f_{\text{K}} - \phi F, \tag{9}$$

where f_{K} is interpreted as the frequency of KRISS-1 seen by the reference oscillator (i.e. hydrogen maser). The frequency measurement made at the west oven can be given as:

$$f_{\text{we}} = f'_{\text{K}} + \phi F'. \tag{10}$$

Assuming that the frequency of the maser is fixed during the beam reversal experiment, $f'_{\text{K}} = f_{\text{K}}$ and the phase difference is given by:

$$\phi = \frac{f_{\text{we}} - f_{\text{ew}}}{F + F'}. \tag{11}$$

The uncertainty in ϕ is from the statistical noise in the frequency measurement and the systematic error in the F-value calculation, which amounts to 0.3 % due to the fact that the field profile in the interaction region is not exactly square. Finally, the frequency of KRISS-1 f_{K} can be obtained from the weighted average:

$$f_{\text{K}} = \frac{F' f_{\text{ew}} + F f_{\text{we}}}{F + F'}. \tag{12}$$

In this calculation the systematic error from F-value becomes negligible because it appears both in the denominator and the numerator. Accordingly, we set the uncertainty in the end-to-end phase bias as the flicker floor level in the frequency stability. For KRISS-1, we have measured the phase difference ϕ of 99.0 μrad. During the operation, we typically measure the frequency shift of 1.171×10^{-12} when the atomic beam flows from east to west or 1.130×10^{-12} when the beam propagates in opposite direction with an uncertainty of 4.1×10^{-15}.

4.8. Bloch-Siegert

In the perturbed Hamiltonian for a two level quantum system interacting with monochromatic coherent field, the time dependent field amplitude carries two oscillation components at ω and $-\omega$. Here the counter-rotating component generates a non-resonant field [22], which does not directly effect the level transition. Although the non-resonant field only shifts the center of Rabi-pedestal, it indirectly influences the center position of the Ramsey spectrum. Bloch-Siegert shift in the central spectrum can be given as:

$$f_{\mathrm{BS}} = \frac{b^2 \Gamma}{16\pi^2 \nu_{\mathrm{hfs}}}, \tag{13}$$

with

$$\Gamma = \frac{1}{D} \int_0^\infty \frac{\partial \Theta}{\partial \Delta_{\mathrm{m}}} \sin^2(\Omega \tau) \sin(\Delta_{\mathrm{m}} T + \Theta) \rho(T) dT. \tag{14}$$

When the oven temperature and the modulation depth are set to 100 °C and 120 Hz respectively, the optimal Rabi-frequency is about 34.0 krad/s and the typical value of Γ is 0.0424. Accordingly, the shift of the Rabi pedestal is 0.796 mHz, and the corresponding frequency shift in Ramsey fringe is 34 μHz. The uncertainty due to the amplitude fluctuation in the microwave and the deduction of the velocity distribution is less than 0.2 %.

4.9. Uncompensated Biases

There are other sources of frequency biases such as light scattering, majorana transition, distributed phase, and vacuum fluctuations inside the atomic beam tube. However, no corrections are made for these parameters because their variations are estimated to be negligible at the level of frequency stability presented in this work. For instance, nonresonant optical transitions caused by stray light may lead to an AC stark effect that shifts the resonance frequency. The stray light can either comes from fluorescent light

emitted by excited atoms or mechanically scattered beams. The fluorescence light shift is calculated to be less than the type-A uncertainty of KRISS-1 based on the theocratical works of Shirley[23], Hisadome [24] and Jun [25] . The mechanical light scattering inside the atomic beam tube has been recently minimized by the insertion of the graphite beam flight tube along the drift region of the cavity. In the experiment, the light scattering was explored by each varying the pump and detection laser power. However, no significant changes in the frequency difference were observed. A conservative uncertainty of 9×10^{-15} is assigned to account for the long term frequency instability of our PFS when the hydrogen maser is used as the reference oscillator.

A propagating atom sees a spatially inhomogeneous magnetic field as a rotating oscillation field, which causes nonadiabatic transitions (Majorana transitions [26]) between magnetic sublevels that have same F quantum number. Majorana transitions may cause a frequency shift if they can create coherence between Zeeman sublevels that are asymmetric with respect to m [14]. In KRISS-1, the magnetic field distribution inside the cavity is very uniform (field inhomogeneity is less than 0.1 %) and the sublevel populations are highly symmetric (asymmetry between the $m = \pm 1$ populations is less than 1 %). Under our experimental conditions, a possible frequency shift less than 1.9×10^{-15} has been estimated based on the study of Bauch and Schroder [27]. And thus this bias has not been corrected and we assign a conservative uncertainty of 2×10^{-15}.

Due to finite conductivity of the cavity, traveling waves give rise to spatial variations in the phase of the microwave field inside the Ramsey cavity. Since the atoms experience a position dependent phase, the resonance frequency depends on the trajectory of the atomic beam. In our experiment, the frequency shifts from this effect was investigated by tuning the beam alignments horizontally, vertically and as well as rotating it about the position of the ovens. Actuators, which are attached at the joint points between

the beam tube and the ovens, provide linear and angular movements with the minimal resolution of 1 μm and 1 μrad. When the actuators are tuned such that the transition signal is maximized, the minimal increment by each actuator corresponds to less than 1×10^{-15} in frequency difference. These tests are found very repeatable, and thus we do not assign any biases for it.

During the continuous operation of KRISS-1, we have noticed rare vacuum spikes that may effect the outcome of the accuracy evaluation. On a random basis, the vacuum level is suddenly raised by about 1.33×10^{-7} Pa and goes back to the previous state within about a minute. We find that such fluctuation in the vacuum condition is correlated to the transition signal strength: Approximately 1.33×10^{-7} Pa increase from the base operating pressure of 1×10^{-6} Pa corresponds to 0.6 % drop in the transition signal. To compensate this effect, the Ramsey signal and the vacuum level are always monitored simultaneously. During the analysis, we omit the data that are taken during the interval of abrupt changes in the vacuum. And also, when the vacuum fluctuation takes place during a Ramsey spectrum scan, the scan is repeated. With these procedures implemented, we did not notice any frequency shift in our data.

5. Frequency Measurement

We ultimately measured f_{K}, which is the frequency of KRISS-1 seen by the hydrogen maser. From the analysis in Eq. (12), the uncertainties in f_{K} are classified to two types: the statistical uncertainty (type-A) in the frequency measurement that is the Allan's deviation in long term, and the systematic uncertainty (type-B) in determining the various frequency biases other than the end-to-end phase bias. The overall performance of our PFS is defined by the combined standard uncertainty of those two.

Fig. 5 shows the Allan deviation of the frequency difference between KRISS-

1 and the hydrogen maser. During the normal operation, KRISS-1 shows a short term frequency stability of $1.3{\times}10^{-12}/\sqrt{\tau}$. Without subtracting the frequency biases investigated in this work, the Allan deviation starts to go up beyond $5{\times}10^4$ s of averaging time and eventually proceeds to exceed $1{\times}10^{-14}$ uncertainty level. However after the periodic biases subtractions, the Allan deviation of $4{\times}10^{-15}$ has been typically measured in one day period (86400 seconds). We note that the Allan deviation from KRISS-1 evetually levels out beyond $2{\times}10^5$ s as can be seen in Fig. 5. This is due to the frequency shift of the reference hydrogen maser.

From July to September of 2008, three sets of accuracy evaluations have been performed. During the same periods, the frequency deviation between our reference H-maser and UTC has also been measured, which can be found in Circular T of BIPM. Using these data, we compared the frequency difference between UTC and our reference H-maser to the frequency difference between KRISS-1 and the maser for three separate occasions: MJD 54654-54669, 54699-54709 and 54719-54739. The validity of the frequency measurement has been checked by the procedure described in following paragraphs.

$$f_1 = f_{KRISS-1} - f_{maser} = f_K, \tag{15}$$

$$f_2 = f_{UTC(KRISS)} - f_{maser}, \tag{16}$$

$$f_3 = f_{UTC} - f_{UTC(KRISS)}. \tag{17}$$

We first measure the frequency difference between KRISS-1 and the reference maser: It is obtained via the data acquisition and analysis procedures that were elaborated in earlier paragraphs. Simultaneously, the frequency difference between the maser and UTC(KRISS) is acquired from our internal time comparison data. Furthermore, the frequency difference between UTC and UTC(KRISS) is obtained from the monthly

updated Circular T. Overall, the comparison between the frequency difference of UTC with respect to KRISS-1 is achieved by comparing f_1 to $f_2 + f_3$.

In Fig. 6, red circles and blue squares represent f_1 and $f_2 + f_3$ in terms of relative frequency respectively. In our measurement, the link uncertainty between UTC(KRISS) and the hydrogen maser is negligible and the accuracy of the data in square is entirely limited by the link uncertainty between UTC and UTC(KRISS), which is reported less than 1×10^{-15} in Circular-T [28]. Nevertheless, we find that the f_1 and $f_2 + f_3$ values are in agreement within 1×10^{-14}. This result implies that the frequency measurement by KRISS-1 conforms to the UTC data within the expected uncertainty. As a preliminary trial, the data was not contributed to TAI, nevertheless, it provides a legitimate test for validating the frequency measurements by our optically pumped atomic clock.

6. Conclusion

In October 2008, we have completed the development of Korea's first PFS. The design and development of all the major components and the method of accuracy evaluation have been accomplished by KRISS personnel. In this work, we find that KRISS-1 and UTC are in good agreement on a consistent basis. In near future, we expect that the frequency measurement by KRISS-1 will contribute to TAI. And also, various theoretical and experimental methods developed in this work will be used to evaluate the performance of atomic fountain clock that is currently under development at KRISS.

7. Acknowledgement

8. References

[1] Vessot R F C, Levine M W, Mattison E M, Blomberg E L, Hoffman T E, Nystrom G U, Farrel B F, Decher R, Eby P B, Baugher C R, Watts J W, Teuber D L and Wills F D 1980 *Phys. Rev. Lett.* **45** 2081

[2] Lemonde P, Laurent P, Simon E, Santarelli G, Clairon A, Salomon C, Dimarcq N and Petit P 1999 *IEEE Trans. Instrum. Meas.* **48** 512

[3] Rawley L A, Taylor J H, Davis M M and Allan D W 1987 *Science* **238** 761

[4] Lee H S, Yang S H, Kim J O, Kim Y B, Baek K J and Kim P S 1998 *Metrologia* **35** 25–31

[5] Park Y H, Lee S H, Park S E, Lee H S and Kwon T Y 2007 *Applied Physics Letter* **90** 174112

[6] Park Y H 2008 Evanescent field paper submitted to JAP

[7] Lee H S, Kwon T Y, Park S E, Choi S K and Park Y H 2004 *Journal of the Korean Physical Society* **45** 256

[8] Kwon T Y, Lee H S, Yang S H and Park S E 2003 *IEEE Transactions on Instrumentation and Measurement* **52** 263–266

[9] Vanier J and Audoin C 1989 *The Quantum Physics of Atomic Frequency Standards* (Bristol and Philadephia, USA: Adam Hilger)

[10] Park S E, Kwon T Y, joo Shin E and Lee H S 2003 *IEEE Transactions on Instrumentation and Measurement* **52** 280–283

[11] Makdissi A and Clercq E D 1997 *IEEE Trans. Ultrason. Ferroelectr. Freq. Control* **44** 637

[12] Shirley J H 1997 *IEEE Trans. Instrum. Meas.* **46** 117

[13] Lee H S, Baek K J, Kwon T Y and Yang S H 1999 *IEEE Transactions on Instrumentation and Measurement* **48** 492–495

[14] Shirley J H, Lee W D and Drullinger R E 2001 *Metrologia* **38** 427

[15] Cutler L S, Flory C A and Giffard R P 1991 *J. Appl. Phys.* **69** 2780

[16] Marchi A D, Rovera G D and Premoli A 1984 *Metrologia* **20** 37

[17] Lee H S, Kwon T Y, Kang H S, Park Y H, Oh C, Park S E, Cho H and Minogin V G 2003 *Metrologia* **40** 224

[18] Park Y H, Oh C H, Kim P S, Kwon T Y, Park S E, Choi S K and Lee H S 2005 *IEEE Transactions on Instrumentation and Measurement* **54** 780

[19] Park Y H 2008 Cavity response paper to be submitted to JAP

[20] Petit G and Wolf P 1997 *IEEE Trans Instrum. Measurement* **46** 201

[21] Pavlis N K and Weiss M A 2003 *Metrologia* **40** 66

[22] Bloch F and Siegert A 1940 *Phys. Rev.* **57** 522

[23] SHIRLEY J H 1985 *Proc. 39th Symposium on Frequency Control* 22–23

[24] Hisadome K 1991 *IEEE Transactions on Ultrasonics. Ferroelectrics. and Frequency Control* **38** 407

[25] Jun J W, Lee H S, Kwon T Y and Minogin V G 2001 *Metrologia* **38** 221–227

[26] Majorana E 1932 *Nuovo Cimento* **9** 43

[27] Bauch A and Schroder R 1993 *Annalen der Physik* **2** 421

[28] Frequency Transfer Uncertainty into TAI, CCTF/06-13, Appendix C
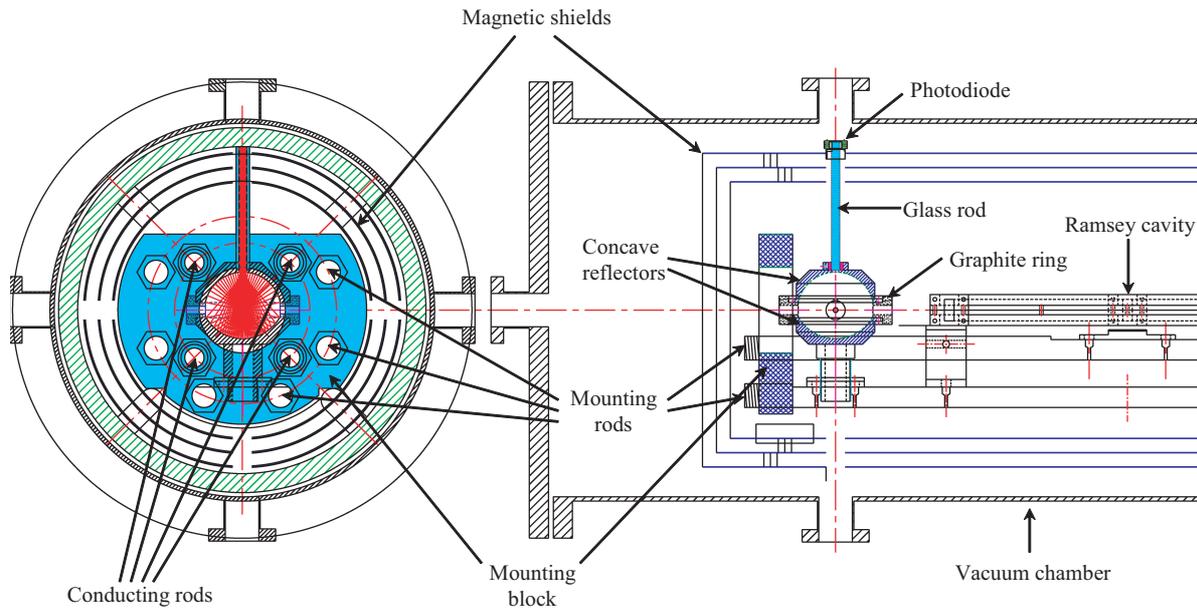
Figure 1. Parts that comprise the atomic clock.
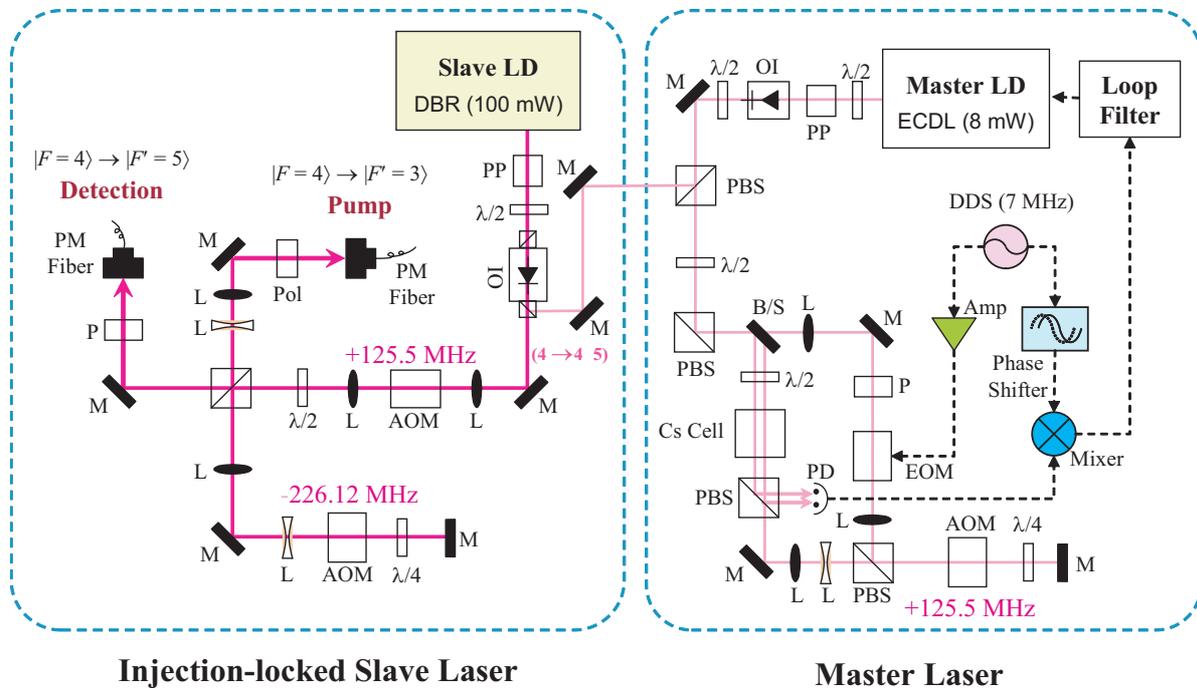
Figure 2. Schematic for the laser system. EOM: electro-optic modulator, AOM: acousto-optic modulator, DDS: direct digital synthesizer, BS: beamsplitter, PBS: polarization beamsplitter, PD: photodiode, PM fiber: polarization maintaining fiber, M: mirror, L: lens, $\frac{\lambda}{2}$: half-wave plate, $\frac{\lambda}{4}$: quarter-wave plate, OI: optical isolator
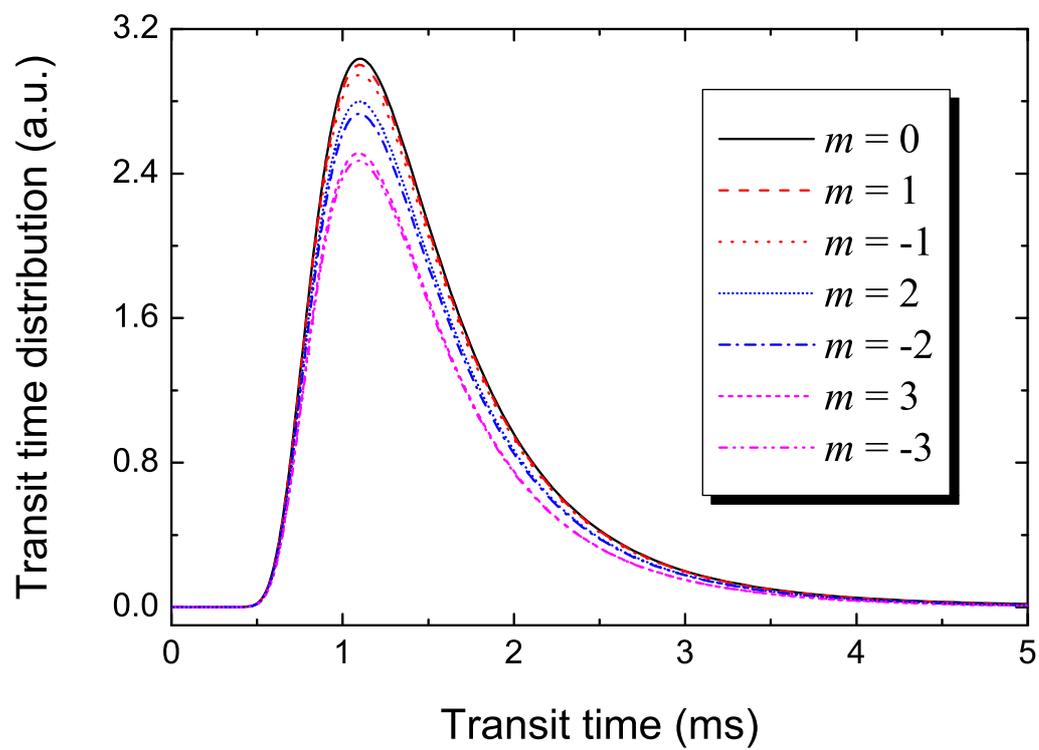
Figure 3. Atomic velocity distributions at m = 0, ±1, ±2, and ±3
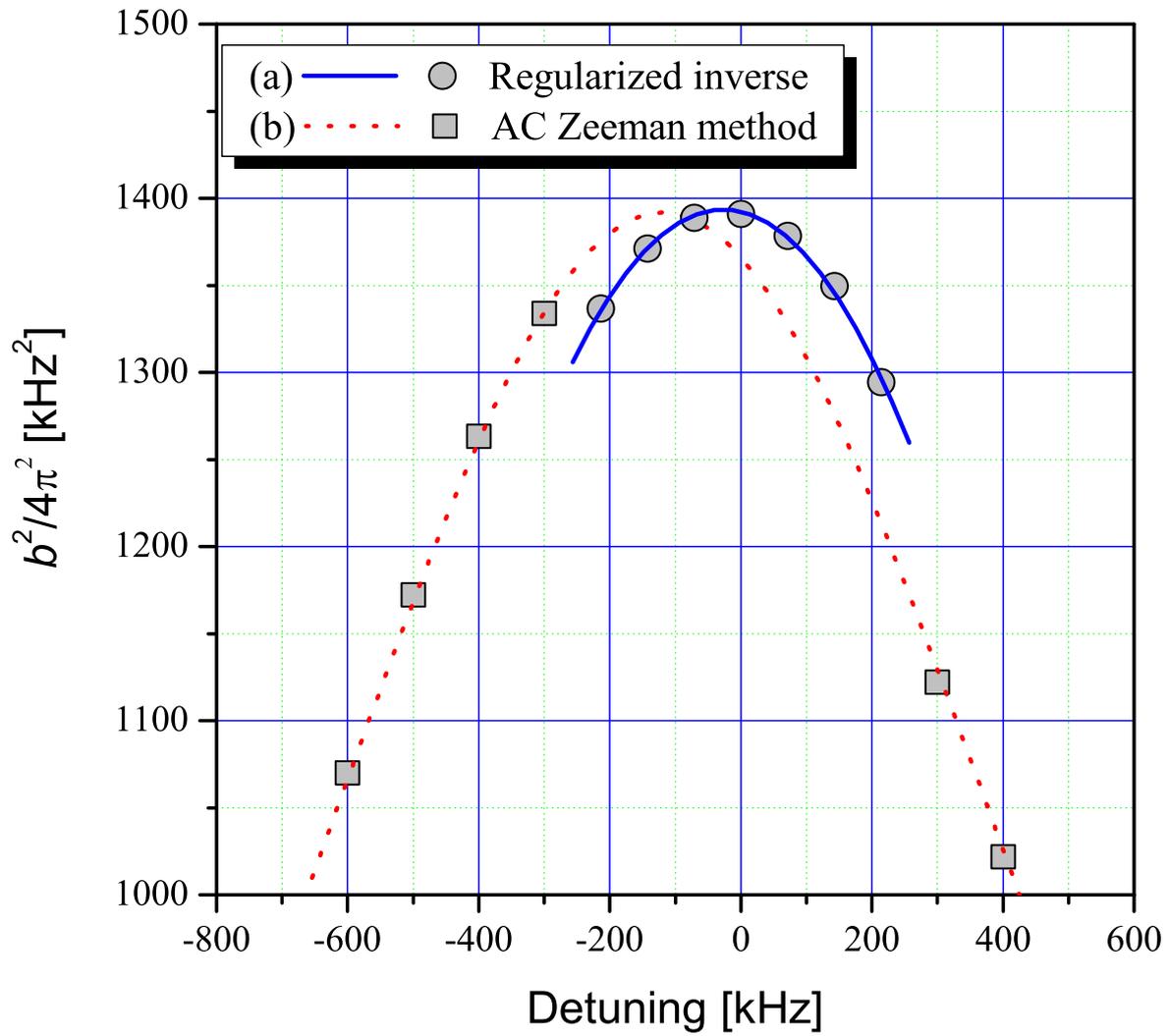
Figure 4. Cavity response function respect to the input microwave frequency. (a) is the response function obtained from a set of 7 Rabi-frequencies measured at m=0, ±1, ±2, and ±3. (b) is the response function obtained from the AC Zeeman method by injecting off-resonant microwave into Ramsey cavity. Two curves are slightly displaced along x-axis because the temperature of the experimental hall was changed by 0.5 °C.
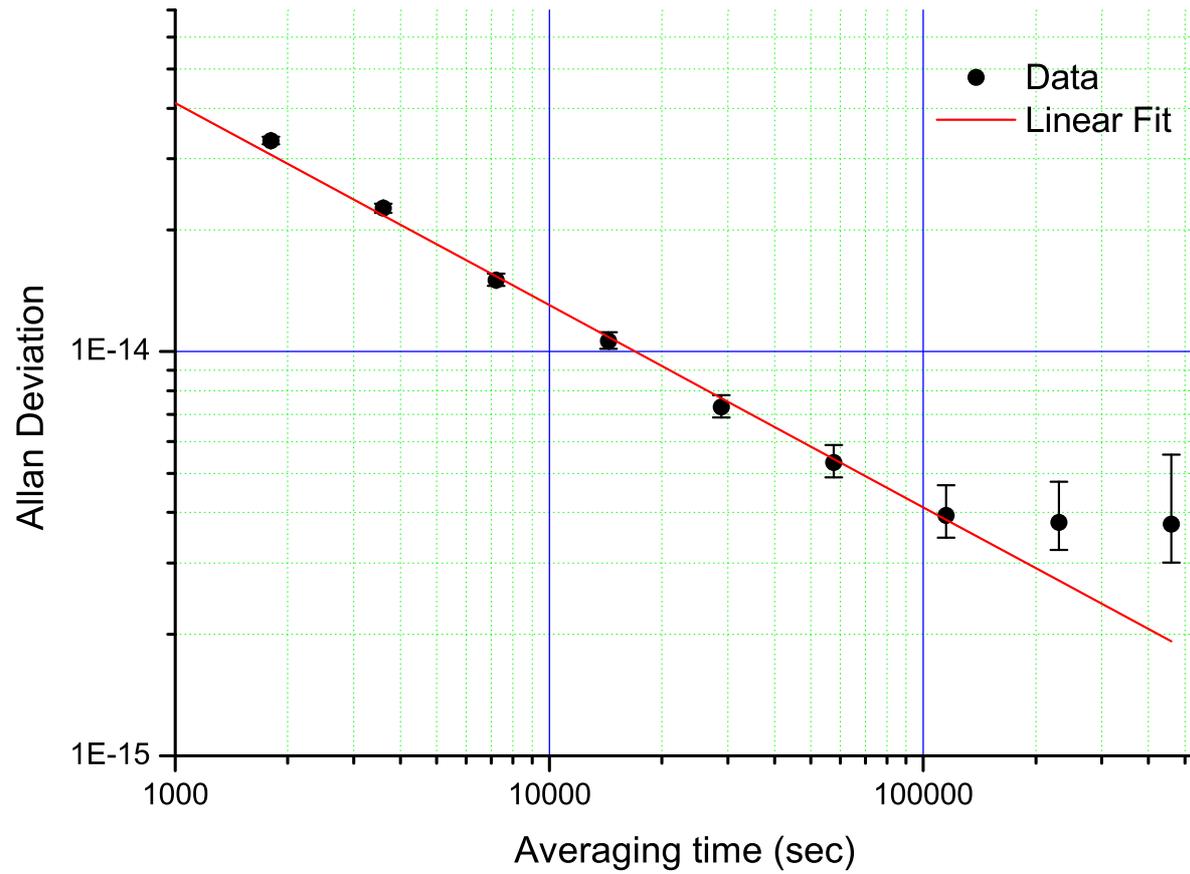
Figure 5. The Allan deviation of the frequency difference between KRISS-1 and the reference maser.
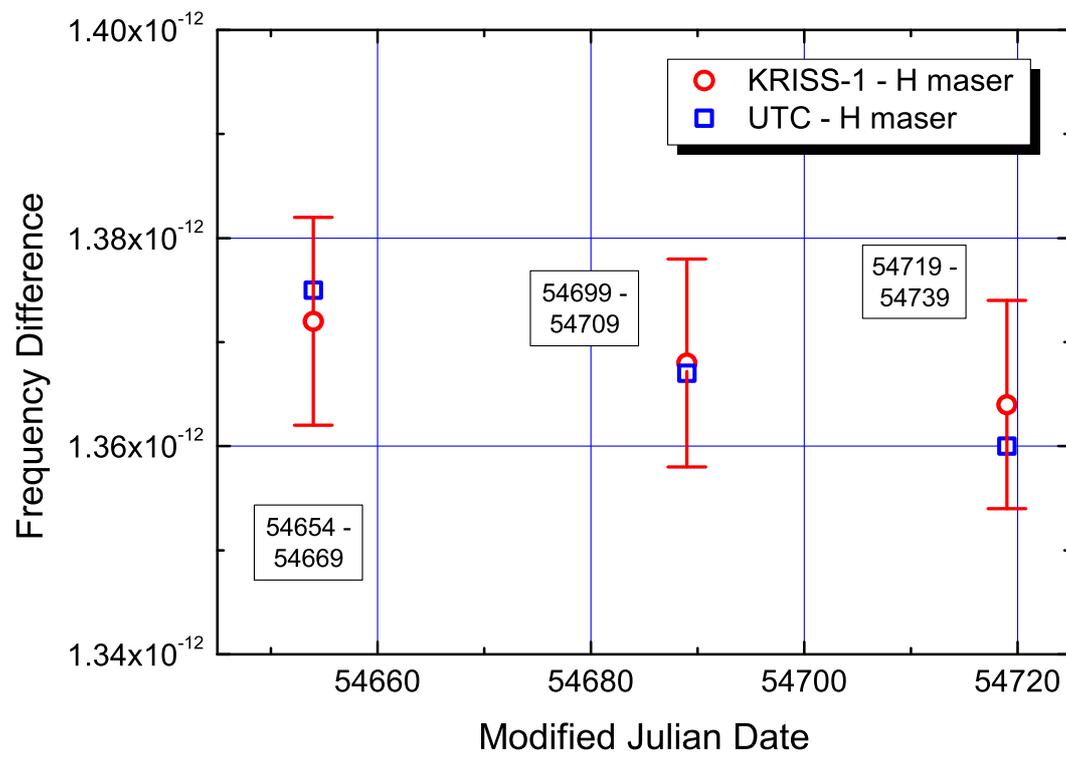
Figure 6. The frequency difference between KRISS-1 and the maser is compared with the frequency difference between the maser and UTC.